Gluon distribution function $xg(x, Q^2)$ and the strong coupling constant $\alpha_s(M_Z^2)$ from the analysis of structure functions

Kunihiro Nagano
on behalf of the H1 and ZEUS collaborations
DESY c/o F1J, Notkestrasse 85, 22603, Hamburg, Germany
E-mail: kunihiro.nagano@desy.de

Abstract. Both the H1 and ZEUS collaborations at HERA have completed new measurements of the neutral-current deep inelastic scattering cross-sections, using data collected in the years 1996 – 1997. Next-to-leading order QCD fits were performed to extract the gluon and quark distribution functions of the proton and the strong coupling constant, $\alpha_s(M_Z^2)$, simultaneously.

1. Introduction

Deep inelastic scattering (DIS) of leptons has been a key tool to probe the structure of the proton. HERA at DESY is a unique facility which collides electrons (or positrons) with protons. The large centre-of-mass energy, $\sqrt{s}$, of about 300 GeV allows an extension of the kinematic phase space by two orders of magnitude both in Q^2, the negative four-momentum transfer squared, and in x, the Bjorken scaling variable. The rapid rise of the proton structure function, $F_2(x, Q^2)$, at low-x observed at HERA [1] continues to generate a lot of interest. Perturbative QCD (pQCD) together with the DGLAP evolution formalism attributes this rapid rise to a large gluon density in the proton.

Recently, both the H1 and ZEUS collaborations completed new measurements of the neutral-current (NC) DIS cross-section, using the e^+p data collected in the years 1996 – 1997 [2, 3], and have performed next-to-leading order (NLO) QCD fits [2, 4]. The parton distribution functions (PDFs) of the proton and the strong coupling constant, $\alpha_s(M_Z^2)$, were extracted simultaneously as will be described in this paper.

2. QCD analysis

2.1. DIS cross-section formulae

The NC cross-section for charged-lepton ($l^\pm$) nucleon (N) DIS can be written as

$$\frac{d^2\sigma^{NC}(l^\pm N)}{dxdQ^2} = \frac{2\pi\alpha^2}{xQ^4}[Y_+F_2^{NC} \mp Y_-xF_3^{NC} - y^2F_L^{NC}], \quad (1)$$

where α is the electromagnetic fine structure constant, y is the inelasticity parameter and $Y_\pm = 1 \pm (1-y)^2$. The structure function (SF) F_3^{NC} is dominated by a parity-violating term and thus makes a significant contribution only at large $Q^2 \gtrsim M_Z^2$, where M_Z is the mass of the Z^0-boson. The longitudinal SF, F_L^{NC}, makes a significant contribution only at large y due to the suppression by the multiplicative y^2 factor. Hence, the NC cross section is dominated by F_2^{NC} at the low-Q^2 and low-y region where most of the precise DIS data lie. Similarly, the charged-current (CC) cross-section for charged-lepton nucleon DIS can be written in terms of SFs as

$$\frac{d^2\sigma^{CC}(l^\pm N)}{dxdQ^2} = \frac{G_F^2}{4\pi x}\frac{M_W^4}{(Q^2+M_W^2)^2}[Y_+F_2^{CC} \mp Y_-xF_3^{CC} - y^2F_L^{CC}], \tag{2}$$

where G_F is the Fermi coupling constant and M_W is the mass of the W-boson. To date, the CC SFs have been most extensively measured in the reverse neutrino and antineutrino DIS reactions.

2.2. QCD fits to DIS data

At the lowest order in pQCD, F_2^{NC} can be written as

$$F_2^p = x[4(u+\overline{u}) + (d+\overline{d}) + (s+\overline{s})]/9, \tag{3}$$

where F_2^p is the proton SF as probed using NC interactions. PDFs are denoted u for the u-quark PDF, $\overline{u}$ for the $\overline{u}$-quark PDF and so on. The strong isospin swapping of F_2^p gives the neutron SF, F_2^n, as

$$F_2^n = x[(u+\overline{u}) + 4(d+\overline{d}) + (s+\overline{s})]/9, \tag{4}$$

which can be obtained from the measured deuteron SF, F_2^D. From the neutrino and antineutrino DIS on isoscalar targets, the CC SFs of the "nucleon" (defined $(p+n)/2$) are measured. These SFs can be written as

$$F_2^{\nu N} = F_2^{\overline{\nu} N} = x[(u+\overline{u}) + (d+\overline{d}) + 2s], \tag{5}$$

$$x[F_3^{\nu N} + F_3^{\overline{\nu} N}]/2 = x[u + d - \overline{u} - \overline{d}] = x[u_V + d_V], \tag{6}$$

where u_V is the valence u-quark PDF and d_V is the valence d-quark PDF. By fitting the DIS SF measurements, PDFs can be extracted. In the H1 and ZEUS QCD fits, the predictions for the SFs were obtained by solving the DGLAP evolution equations at NLO in the $\overline{\mathrm{MS}}$ scheme.

2.3. Highlights of the H1 and ZEUS NLO-QCD fits

2.3.1. New precise HERA structure function measurements: Given the increased amount of luminosity (about 30 pb^{-1}) the new F_2 measurements from H1 and ZEUS are significantly more precise than the previous measurements using the 1994 data (about 2 pb^{-1}) [1]. In addition, the improved understanding of the detectors allowed an extension of the kinematic phase space, especially in the low-y and high-y regions. For example, the newly installed small-angle tracking device of the H1 detector has allowed a better position reconstruction for the positrons at small scattering angle. In the ZEUS measurement, the hadronic system is reconstructed better by combining both tracking and calorimeter measurements, and the positron energy is corrected cell-by-cell. The kinematic region covered is $Q^2 > 1.5$ GeV^2 by H1 and $Q^2 > 2.7$ GeV^2 by ZEUS with a typical precision of 1% for the statistical errors and of 3% for the systematic uncertainties. The wide Q^2 range covered enables a simultaneous extraction of $\alpha_s(M_Z^2)$ and the gluon PDF, $xg(x, Q^2)$, from the scaling violations of F_2, and the improved precision requires QCD fits to take the experimental systematic uncertainties into account. These two items are discussed in the following subsections.

2.3.2. Simultaneous extraction both of $\alpha_s(M_Z^2)$ and PDFs: In pQCD, the scaling violations are caused by gluon bremsstrahlung from quarks and quark-antiquark pair creation from gluons. At low-x, the scaling violations are driven mainly by the latter. Hence, the scaling violations of F_2 are sensitive to α_s and xg. Therefore, given the precise HERA data, a simultaneous extraction both of $xg(x, Q^2)$ and $\alpha_s(M_Z^2)$ can be made by a fit in which both PDFs and $\alpha_s(M_Z^2)$ are free. Notice also that the correlation between the PDFs and $\alpha_s(M_Z^2)$ can be considered in such fits.

2.3.3. Sophisticated treatment of correlated experimental systematic uncertainties: The systematic uncertainty dominates at low $Q^2 \lesssim 1000$ GeV^2 in the new HERA measurements. Such experimental systematic uncertainties were handled taking the point-to-point correlations of the uncertainties fully into account [5]. A χ^2 is defined as

$$\chi^2 \equiv \sum_i^{data} \frac{(t_i(p)/f_i(s) - m_i)^2}{(\delta_i^{stat})^2 + (\delta_i^{uncor.syst})^2} + \sum_l^{syst.source} (s_l)^2, \tag{7}$$

$$f_i = 1 + \sum_l^{syst.source} \beta_{il} s_l, \tag{8}$$

where t_i and m_i represent the QCD prediction and measured value at kinematic point i, respectively. The δ_i^{stat} and $\delta_i^{uncor.syst}$ represent the statistical and uncorrelated systematic uncertainties of the measurement at kinematic point i. The symbol p denotes the set of fitted PDF parameters, while s_l is the systematic uncertainty parameter assigned to the correlated systematic uncertainty source l and β_{il} represents the fractional error of source l at kinematic point i. The systematic parameters s are left free in the H1 NLO-QCD fit, and are set to zero in the ZEUS NLO-QCD fit. For more detailed explanations of this systematic uncertainty treatment, see the comprehensive review contributed to this workshop [6].

3. H1 NLO-QCD fit

The H1 analysis [2] stresses extracting $xg(x, Q^2)$ and $\alpha_s(M_Z^2)$ by fully exploiting the sensitivity of their data. The analysis was made only on proton target data, namely H1 data together with the BCDMS muon-proton DIS cross-section data [7]. This means that the deuterium-target DIS measurements were not used and so uncertainties in the nuclear correction for deuterium can be avoided.

The flavour decomposition of F_2 was minimal; i.e. only two independent quark distribution functions were used. This is because there is not sufficient sensitivity for example to the d-quark PDF when only proton-target data are used (see (3)). A new flavour decomposition was invented; the "valence-quark", $V(x,Q^2)$, and "sea quark", $A(x,Q^2)$, functions are defined as

$$V \equiv \frac{3}{4}\cdot\frac{1}{1+\epsilon}[(3+2\epsilon)u_V - 2d_V + (5+2\epsilon)(\overline{u}-\overline{d})], \tag{9}$$

$$A \equiv \frac{1}{4}\cdot\frac{1}{1+\epsilon}[(4\overline{u} - (u_V - 2d_V) - 5(\overline{u}-\overline{d}) + 2\epsilon(\overline{u}-\overline{d})], \tag{10}$$

where the s-quark contribution is expressed with ϵ defined as $s+\overline{s} \equiv (\frac{1}{2}+\epsilon)\cdot(\overline{u}+\overline{d})$. The NuTeV measurement of ϵ based on muon production in CC neutrino-nucleon interactions, $\epsilon = -0.08$, was used [8]. Compared to using e.g. the singlet and non-singlet functions $\Sigma \equiv U+D$ and $\Delta \equiv 2U-D$ to decompose F_2 ($U \equiv u+\overline{u}, D \equiv d+\overline{d}+s+\overline{s}$), the new decomposition with V and A has the advantage that V can be constrained by the quark number sum-rule: $\int_0^1 V dx = 3+\delta\cdot\frac{3}{4}\cdot\frac{5+2\epsilon}{1+\epsilon}$, where $\delta \equiv \int_0^1(\overline{d}-\overline{u})dx$. The E866/NuSea measurement on the Drell-Yan muon-pair production at the Tevatron, $\delta = -0.118$ at $Q^2 = 54$ GeV^2, was used [9]. The H1 fit gave a value of $\int_0^1 V dx = 2.24 \pm 0.13(exp.)$ if this constraint was removed. Also, the momentum sum-rule was imposed. $V(x)$ and $A(x)$ together with $g(x)$ were parameterised at $Q_0^2 = 4$ GeV^2. The functional form for these PDFs is taken to be: $ax^b(1-x)^c(1+d\sqrt{x}+ex)$, where $(1+d\sqrt{x}+ex)$ is called the smoothing function. There are 13 free PDF parameters and 21 variable systematic parameters. For heavy-quark (c- and b-quark) production, the fixed-flavour number scheme (FFN) was used. The heavy-quarks are dynamically produced via the boson-gluon-fusion process ($\gamma^* g \to c\overline{c}$) in this scheme.

Two fits were made; one using both H1 and BCDMS data to determine $\alpha_s(M_Z^2)$ and PDFs simultaneously, and the other using H1 data alone to determine the gluon PDF. A cut of $Q^2_{\rm min} = 3.5$ GeV^2 was applied. Also, the requirement $Q^2 < 3000$ GeV^2 was applied to eliminate the kinematic region where the xF_3 contribution is sizeable. A cut of $x_{\rm min} = 3\cdot 10^{-4}$ was applied. In addition, a cut of $y > 0.3$ was applied for the BCDMS data to avoid regions of large systematic uncertainties.

3.1. Determination of $\alpha_s(M_Z^2)$ and PDFs

The fit to the H1 and BCDMS data sets leaving $\alpha_s(M_Z^2)$ as a free parameter (denoted "H1+BCDMS fit") resulted in a χ^2/dof of 394/451. Figure 1 shows F_2 determined from the H1+BCDMS fit together with the data that were used in the fit. The H1+BCDMS fit describes the scaling violations well. The value of $\alpha_s(M_Z^2)$ extracted is

$$\alpha_s(M_Z^2) = 0.1150 \pm 0.0017(exp)^{+0.0009}_{-0.0005}(model). \tag{11}$$

The first error arises from the experimental statistical and correlated systematic uncertainties. The second error is the "model error" which arises from uncertainties

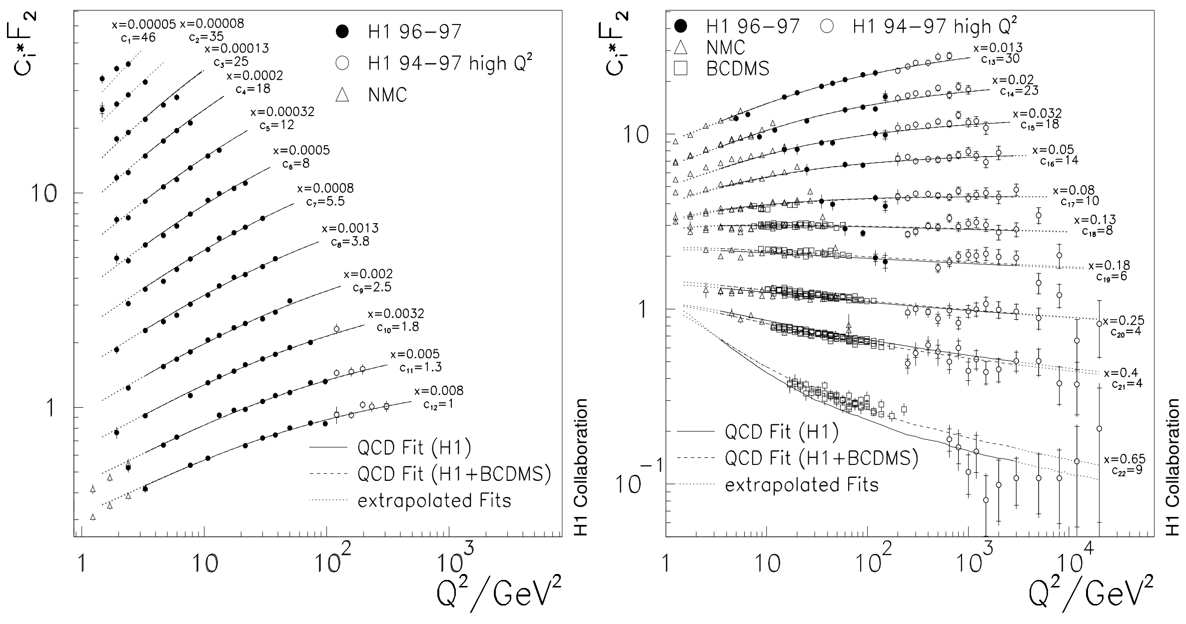

Figure 1. F_2 by the H1 NLO-QCD fit compared to data from H1 and BCDMS.

in various fit assumptions. For example, the $Q^2_{\rm min}$ threshold, the Q_0^2 value, and the masses of charm (m_c) and bottom (m_b) quarks were varied. Also, the model error due to the parameterisation of the PDFs was evaluated by reducing or adding parameters for the smoothing function. The variations of the $x_{\rm min}$ threshold and m_c were found to give the largest contribution to the model error on the extracted value of $\alpha_s(M_Z^2)$. In addition to the model error, the scale uncertainty was evaluated by changing the renormalisation (μ_R^2) and factorisation scales (μ_F^2) from Q^2 to $Q^2/4$ and $4Q^2$. A large shift of 0.005 was observed in the extracted $\alpha_s(M_Z^2)$ value. This indicates that the next-to-NLO (NNLO) correction is important in the extraction of $\alpha_s(M_Z^2)$ from the scaling violations of F_2.

The α_s extraction was repeated using H1 data alone and using BCDMS data alone. Figure 2 shows the χ^2 increase from its minimum as a function of $\alpha_s(M_Z^2)$ for each of these fits. The fit to H1 data alone gave $\alpha_s(M_Z^2) = 0.115 \pm 0.005(exp.)$, which is consistent with that obtained by the H1+BCDMS fit. However, the fit to BCDMS alone gave a small $\alpha_s(M_Z^2)$ value of 0.111. This was found to be due to a negative correlation between $\alpha_s(M_Z^2)$ and the b-parameter of $g(x)$ PDF which yields the low-x behaviour. This caused a small $\alpha_s(M_Z^2)$ and a positive b-parameter, i.e. a flat behaviour at low-x for $xg(x, Q^2)$. In summary, the HERA data provide $xg(x, Q^2)$ at low-x and determine $\alpha_s(M_Z^2)$.

3.2. Determination of $xg(x, Q^2)$

A fit was performed to H1 data alone (denoted "H1 fit") with a fixed $\alpha_s(M_Z^2)$ value of 0.115 as determined by the H1+BCDMS fit. Figure 3 shows the $xg(x, Q^2)$ distribution.

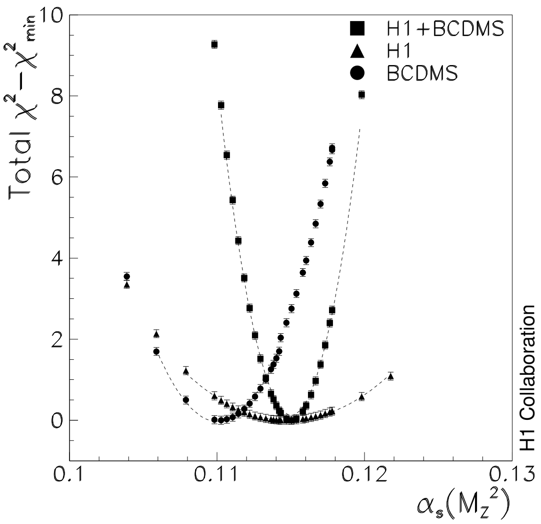

Figure 2. χ^2 increase for the three $\alpha_s(M_Z^2)$ extractions using: H1+BCDMS, H1 alone and BCDMS alone, respectively.

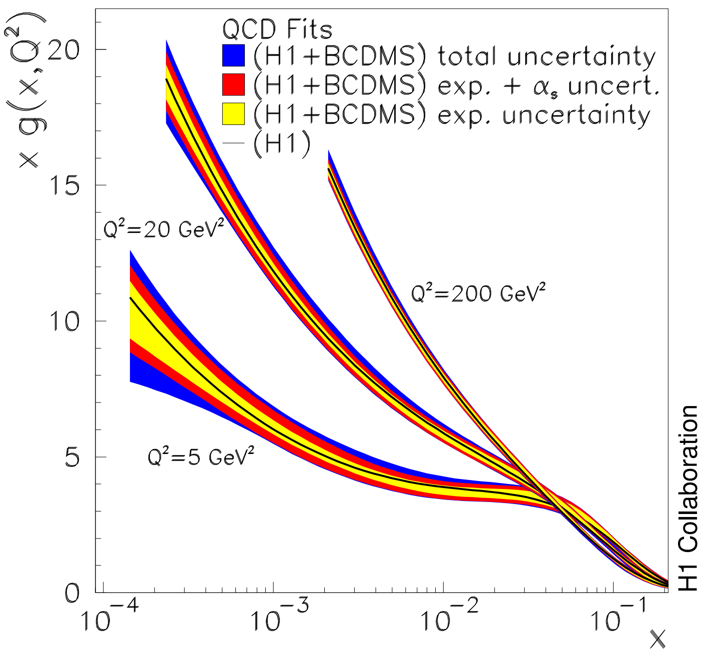

Figure 3. $xg(x, Q^2)$ by the H1 NLO-QCD fit.

The curve represents the H1 fit and the three error-bands represent the uncertainties evaluated from the H1+BCDMS fit; both fits agree well. The inner-most error-band represents the uncertainties due to experimental errors as evaluated by the H1+BCDMS fit but fixing $\alpha_s(M_Z^2) = 0.115$. The second error-band represents the uncertainties as evaluated from the H1+BCDMS fit which leaves $\alpha_s(M_Z^2)$ as a free parameter. Note that the errors on xg evaluated in this way can be considered to include the α_s uncertainty. The outer-most error-band shows the total uncertainties with the model errors added

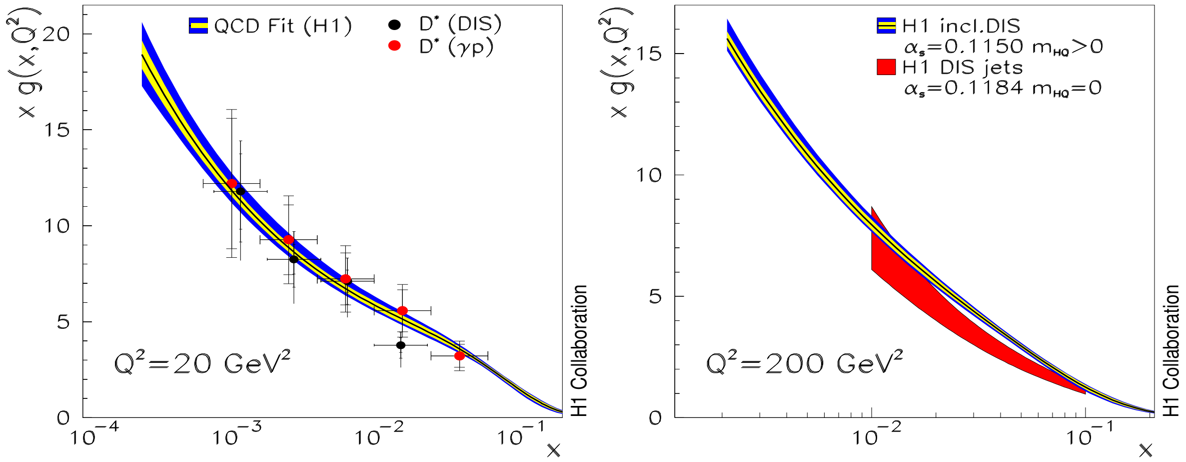

Figure 4. $xg(x, Q^2)$ by the H1 NLO-QCD fit compared to other H1 measurements; (left) from D^* production both in DIS and γP interactions, (right) from DIS jets.

in quadrature. The largest model error was found to be due to the $Q^2_{\rm min}$ threshold and the m_c. Other checks, e.g. on Q^2_0, were found to give small effects. Also, the zero-mass variable-flavour number (ZM-VFN) scheme was tried for heavy-quark production, in which heavy quarks are active with zero-mass when Q^2 exceeds the mass threshold. The difference between the FFN and ZM-VFN schemes was found be large at low $x \lesssim 10^{-2}$; generally ZM-VFN gives a smaller $xg(x, Q^2)$ (not included in the model error).

Figure 4 shows $xg(x, Q^2)$ compared to that extracted from D^* production in DIS and γp interactions [10], which are sensitive to xg as $\gamma(^*)g \rightarrow c\bar{c}$. As shown, the xg extracted in this analysis is more precise than, and is consistent with, that from the D^* analyses. Figure 4 also shows $xg(x, Q^2)$ compared to that extracted from DIS jets [11]. Both are in good agreement in general. However, there is a small difference at $10^{-2} \lesssim x \lesssim 10^{-1}$. It may be understood in terms of the extra constraint of xg at high-x in the DIS jet analysis. Note also that the heavy-quark treatments are different in the DIS jet analysis (ZM-VFN) and the current analysis (FFN).

It is also worth noting that F_L, which is strongly sensitive to xg, was extracted in a model-independent way. The F_L expectation of the NLO-QCD fit agrees well with the measurement, which provides a good check on the xg extraction. For more details, see the review contributed to this workshop [12].

4. ZEUS NLO-QCD fit

The ZEUS analysis [4] aims at extracting $\alpha_s(M_Z^2)$ and the PDFs in a standard, 'MRS-like', flavour decomposition by fully exploiting the sensitivity of both ZEUS and fixed-target DIS data. Notice that the PDFs in a standard flavour decomposition can be straightforwardly used also for other processes. The precise fixed-target data sets with full correlated systematic uncertainties available were used. The proton SF F_2^p data from BCDMS [7], NMC [13] and E665 [14] were used. To increase the sensitivity to the d-quark (see section 2.2), the deuteron SF F_2^D data from NMC [13] and E665 [14] were used. The ratio F_2^D/F_2^p from NMC [15] was also used. It is particularly important for the determination of the shapes of the u- and d-valence quark PDFs. In addition, the nucleon SF data from CCFR [16] using a neutrino-beam were used. Only $xF_3^{\nu N}$, which is sensitive to the u- and d-valence PDFs (see section 2.2), was used. A cut of $Q^2 > 2.5$ GeV^2 was applied. Also, a cut of $W^2 > 20$ GeV^2 was made to avoid possible target-mass and higher-twist effects. In total, 1263 (242 from ZEUS) data points were used. There are 71 correlated experimental systematic uncertainties in total, all of which were taken into account with the method described in section 2.3.3.

The PDFs were parameterised at $Q_0^2 = 7$ GeV^2 for the u- and d-valence quarks, sea-quarks and gluon. The s-quark contribution to the (total) sea-quark PDF is assumed to be 20%, which is consistent with the CCFR measurement [17]. The difference between the $\overline{d}$- and $\overline{u}$-quark distributions was also parameterised. The form for the PDFs was taken to be: $p_1 x^{p_2}(1-x)^{p_3}(1+p_4\sqrt{x}+p_5 x)$. Some parameters were fixed; firstly, p_4 was set equal to zero for all PDFs. They describe the high-x behaviour of PDFs and cannot be constrained sufficiently by DIS data, giving a large correlation to other parameters if they are left free. For xg, p_5 was also fixed at zero. For the u- and d-valence PDFs, p_2 was fixed at 0.5, since there is not enough information on low-x valence shapes without using e.g. $W^\pm$-asymmetry data from the Tevatron. For the $(\overline{d}-\overline{u})$ PDF, only the normalisation parameter p_1 was free. The number sum-rules for the u-valence and d-valence PDFs were imposed, respectively. The momentum sum-rule was also imposed. In total, 11 parameters were free. For heavy-quark production, a general mass variable-flavour-scheme (RT-VFN) was used [18]. The FFN scheme is suitable at Q^2 close to the mass threshold; however, is not suitable at large Q^2 due to the neglected $\ln(Q^2/m_c^2)$ terms. In contrast, the ZM-VFN scheme is suitable at large Q^2 since such terms are re-summed in the heavy-quark PDFs. However, the ZM-VFN scheme is apparently not suitable for Q^2 close to the mass threshold. The RT-VFN scheme can be regarded as a practical solution for a smooth combination of the FFN and ZM-VFN schemes and, hence, can be applied in a wide range of Q^2.

4.1. Results of the ZEUS NLO-QCD fit

The central fit was performed by fixing $\alpha_s(M_Z^2)$ at the world average value of 0.118 [19]. Figure 5 shows F_2 by the fit compared to the experimental data. The fit yields a good description of both ZEUS and fixed-target data. The χ^2 value, divided by the number of data points, was 0.95 for all and 0.85 for ZEUS (the numbers were calculated by adding statistical and systematic uncertainties in quadrature).

Figure 6 shows $xg(x, Q^2)$. The uncertainties are indicated separately for those due to statistical errors and uncorrelated systematic uncertainties and for those correlated systematic uncertainties added in quadrature (denoted “total”). Also shown is the uncertainty estimated by the fit taking $\alpha_s(M_Z^2)$ as a free parameter (see later in section 4.2). This gives an estimation of the PDF error due to the uncertainty in α_s.

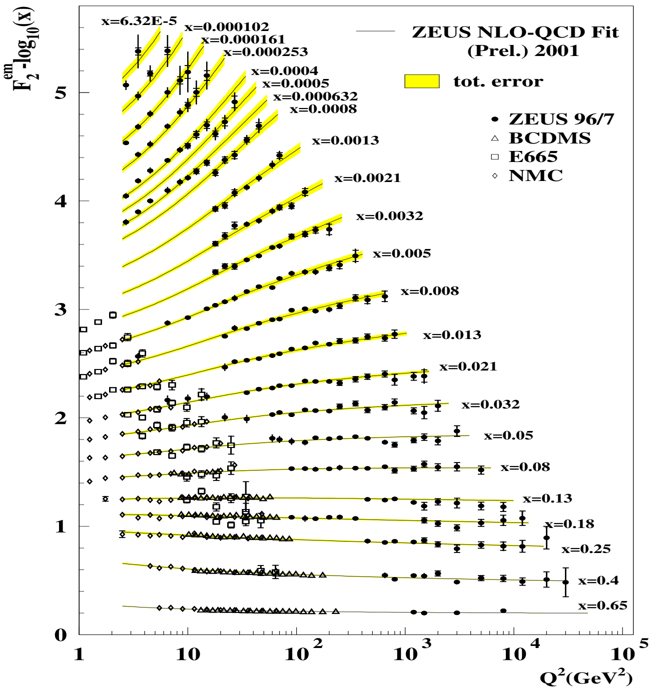

Figure 5. F_2 by the ZEUS NLO-QCD fit compared to data from ZEUS and fixed-target experiments.

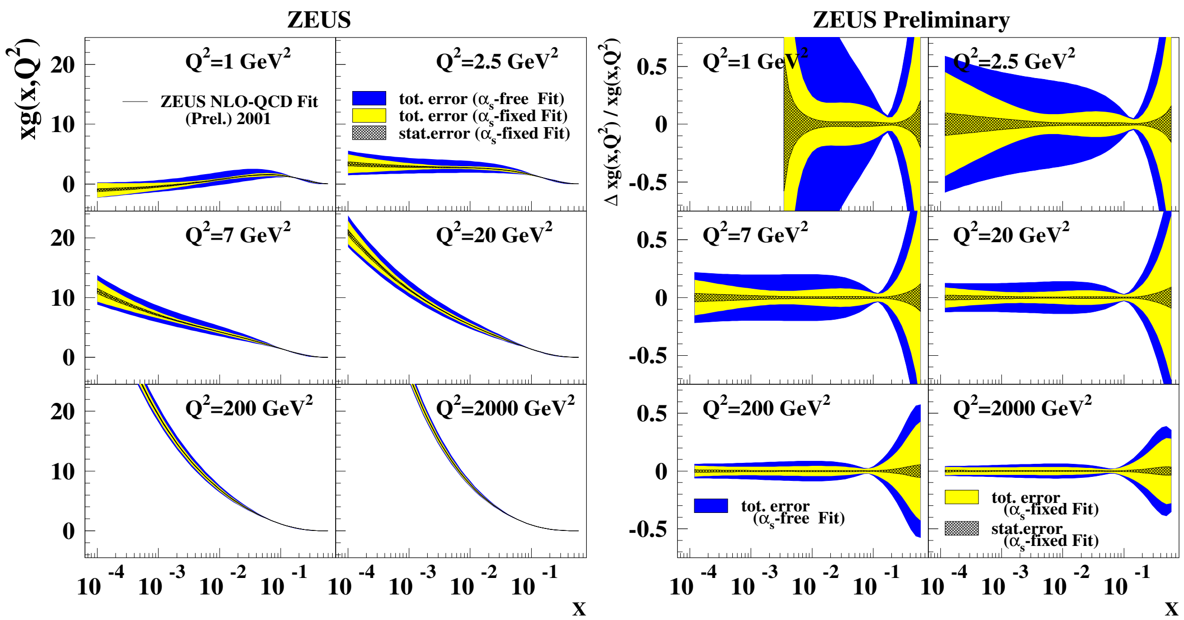

Figure 6. $xg(x, Q^2)$ by the ZEUS NLO-QCD fit: (left) absolute value, (right) relative uncertainty.

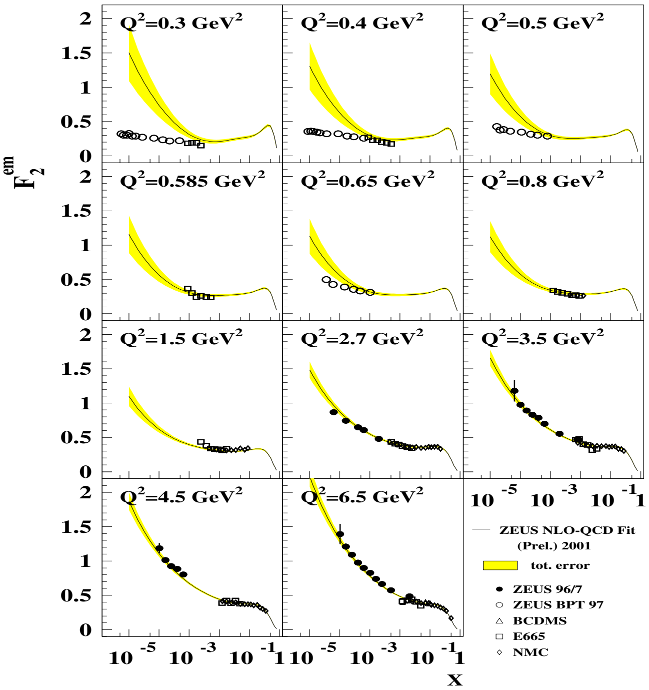

Figure 7. F_2 by the ZEUS NLO-QCD fit extrapolated down to very low Q^2 compared to experimental data.

It can be seen that the uncertainty is typically $\sim 10\%$, growing larger at $x \gtrsim 0.1$. This is because of the lack of experimental data sensitive to the high-x gluon, a challenge common to this type of QCD analysis of proton PDFs [20]. An interesting feature of the extracted xg is the valence-like behaviour at very low $Q^2 \sim 1$ GeV^2, which may be related to the issue of the limit of applicability of pQCD as described below. The sea-quark PDF was determined with a typical uncertainty of 5%. Interestingly, the sea-quark PDF shows a slight rise even at $Q^2 \sim 1$ GeV^2. The u-valence PDF was determined with a few % precision up to a very large x of about 0.6. The uncertainty of the d-valence PDF was larger than that of the u-valence PDF, reflecting $F_2^D \propto x(u_V + d_V)$ while $F_2^p \propto x(4u_V + d_V)$ at large-x (see section 2.2).

Figure 7 shows F_2 extrapolated down to the very low-$Q^2 \sim 0.3$ GeV^2 region. The NLO-QCD fit overshoots ZEUS BPT data [21] which lie at $x \lesssim 10^{-2}$ and $Q^2 < 0.65$ GeV^2. In this region, the F_L predicted by the NLO-QCD fit was found to be negative. This may also indicate that the DGLAP pQCD approach cannot be applied below $Q^2 \sim 1$ GeV^2.

To see the sensitivity of the ZEUS data, two special fits were performed: one without using ZEUS data and the other using only ZEUS data. The fit without ZEUS data resulted in almost flat gluon and sea-quark PDFs at Q_0^2 with a much larger uncertainty. Recall that the flat xg was also observed in H1's fit using BCDMS data alone with $\alpha_s(M_Z^2)$ free (see section 3.1). This shows that the HERA data determine the low-x behaviour of the gluon and sea-quark PDFs. In the fit using only ZEUS data (denoted

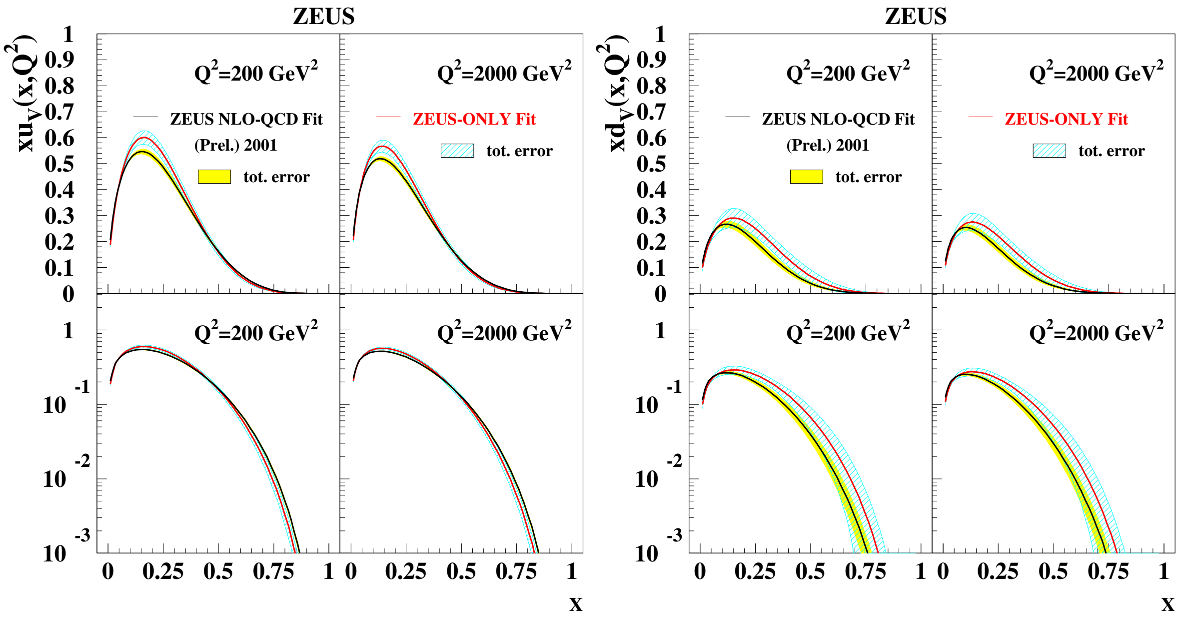

Figure 8. Valence quark PDFs from the ZEUS-only fit: (left) u-valence PDF, (right) d-valence PDF.

ZEUS-only fit), NC and CC cross-sections for both e^-p and e^+p DIS were used [22]. Figure 8 shows the u- and d-valence PDFs determined by the ZEUS-only fit. As clearly demonstrated, the HERA data have a sensitivity to determine even the valence PDFs with a reasonable precision. Also it is interesting that the ZEUS data prefer more u-valence quark at middle $x \sim 0.1$, but fewer u-valence quark at large $x \gtrsim 0.7$, than that preferred by the global fit to ZEUS and fixed-target experimental data. In contrast, the ZEUS data prefer more d-valence quark with a small shift of the peak of the d-valence PDF.

4.2. Extraction of $\alpha_s(M_Z^2)$

Another fit, in which $\alpha_s(M_Z^2)$ is treated as a free parameter, was performed to determine both the PDFs and $\alpha_s(M_Z^2)$ simultaneously. The fit yielded

$$\alpha_s(M_Z^2) = 0.1172 \pm 0.0008(stat. + uncor.syst.) \pm 0.0054(syst.),$$

where the errors are due to statistical and uncorrelated systematic uncertainties, and correlated systematic uncertainties, respectively. The value is consistent with the world average of 0.118. The value is also consistent with the ZEUS measurement from the di-jet ratio in NC DIS events [23].

A large uncertainty was obtained due to the full accounting of the correlated systematic errors. This covers the variation from the traditional lower values of $\alpha_s(M_Z^2)$ determined from fixed-target DIS data, e.g. $\alpha_s(M_Z^2) = 0.113$ from BCDMS [24], to the higher values favoured by LEP data, $\alpha_s(M_Z^2) = 0.120$ [25]. However, the H1 NLO-QCD fit evaluates a smaller error of 0.0017 on $\alpha_s(M_Z^2)$ due to the experimental errors (see

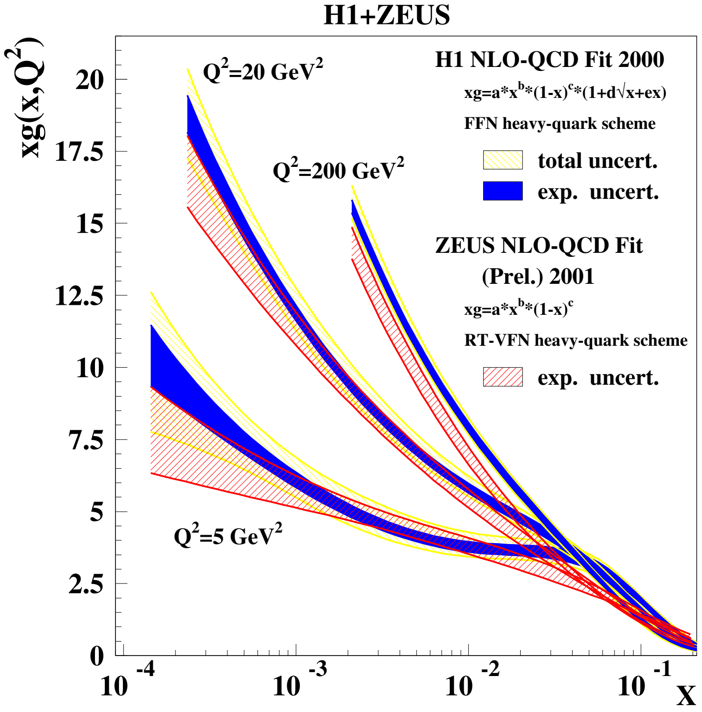

Figure 9. A combined plot of $xg(x, Q^2)$ for the H1 and ZEUS NLO-QCD fits.

(11)). This is due to the different treatment of the correlated systematic uncertainties (H1 fits the systematic parameters, while ZEUS does not, see section 2.3.3). This matter is under investigation.

5. Conclusion

Figure 9 shows a combined plot of $xg(x, Q^2)$ from the H1 and ZEUS NLO-QCD fits. It can be seen that both are in reasonable agreement. However, there are three major differences in the xg distribution which may be attributed to the differences in the analyses. The first difference is in the shape of xg at middle-x, $10^{-2} \lesssim x \lesssim 10^{-1}$. This may be due to the different parameterisation; the H1 analysis used $ax^b(1-x)^c(1+d\sqrt{x}+ex)$ and the ZEUS analysis used $ax^b(1-x)^c$. The second difference is the slope of xg; the ZEUS xg is less steep than the H1 xg, in general. This can be understood as being due to the different heavy-quark production schemes. The last difference is the size of the uncertainty, as already pointed out for the $\alpha_s(M_Z^2)$ extraction in section 4.2. This may be due to the different treatment of the correlated systematic uncertainties. Investigations to clarify these differences are currently undertaken by the two experiments.

References

[1] S. Aid *et al.*, H1 Collaboration, *Nucl. Phys.* B **470**, 4 (1996);
M. Derrick *et al.*, ZEUS Collaboration, *Z. Phys.* C **72**, 399 (1996).
[2] C. Adloff *et al.*, H1 Collaboration, *Eur. Phys. J.* **21**, 33 (2001).
[3] S. Chekanov *et al.*, ZEUS Collaboration, DESY-01-064, accepted by *Eur. Phys. J.*
[4] ZEUS Collaboration (prel.), contributed paper 628 to EPS HEP 2001.
[5] C. Pascaud and F. Zomer, LAL 95-06.
[6] M. Botje, talk given at this workshop, article elsewhere in these proceedings.
[7] A.C. Benvenuti *et al.*, BCDMS Collaboration, *Phys. Lett.* B **223**, 485 (1989).
[8] T. Adams *et al.*, NuTeV Collaboration, hep-ex/9906038(1999).
[9] E.A. Hawker *et al.*, E866/NuSea Collaboration, *Phys. Rev. Lett.* **80**, 3715 (1998).
[10] C. Adloff *et al.*, H1 Collaboration, *Nucl. Phys.* B **545**, 21 (1999).
[11] C. Adloff *et al.*, H1 Collaboration, *Eur. Phys. J.* **C19**, 289 (2001).
[12] N. Gogitidze, talk given at this workshop, article elsewhere in these proceedings.
[13] M. Arneodo *et al.*, NMC Collaboration, *Nucl. Phys.* B **483**, 3 (1997).
[14] M.R. Adams *et al.*, E665 Collaboration, *Phys. Rev.* D **54**, 3006 (1996).
[15] M. Arneodo *et al.*, NMC Collaboration, *Nucl. Phys.* B **487**, 3 (1997).
[16] W.G. Seligman *et al.*, CCFR Collaboration, *Phys. Rev. Lett.* **79**, 1213 (1997).
[17] A.O. Bazarko *et al.*, CCFR Collaboration, *Z. Phys.* C **65**, 189 (1995).
[18] R. Thorne and R.G. Roberts, *Phys. Rev.* D **57**, 6871 (1998).
[19] S. Bethke, J.Phys. **G26**, R27 (2000).
[20] see e.g. S. Kuhlmann *et al.*, *Phys. Lett.* B **476**, 291 (2000).
[21] J. Breitweg *et al.*, ZEUS Collaboration, *Phys. Lett.* B **487**, 53 (2000).
[22] ZEUS Collaboration (prel.), contributed paper 413 and 414 to ICHEP 2000;
ZEUS Collaboration, *Eur. Phys. J.* **C12**, 411 (2000).
[23] J. Breitweg *et al.*, ZEUS Collaboration, *Phys. Lett.* B **507**, 70 (2001).
[24] M. Virchaux and A. Milsztajn, *Phys. Lett.* B **274**, 221 (1992).
[25] D.E. Groom *et al.*, Particle Data Group, *Eur. Phys. J.* **C15**, 1 (2000).